

Paper:

Design of Vertebrae-Inspired Trunk Mechanism for Robust and Directive Quadruped Locomotion on Rough Terrain Without Requiring Sensing and Actuation

Takashi Takuma, Yoshiki Murata, and Wataru Kase

Osaka Institute of Technology

5-16-1 Omiya, Asahi-ku, Osaka 535-8585, Japan

E-mail: takashi.takuma@oit.ac.jp

[Received November 28, 2016; accepted April 26, 2017]

Quadrupedal animals adaptively change their trunk posture in order to avoid falling down and to facilitate directive locomotion even on rough terrain. This paper focuses on an animal-like trunk mechanism which has passive viscoelastic joints. The effect of the trunk mechanism is observed by changing the elasticity and configuration of joints. Simulation results showed that the locomotion success rate of a robot equipped with the trunk mechanism on rough terrain is higher than the locomotion success rate of a robot equipped with a rigid body. In addition, the distribution of the success rate changes according to the elastic coefficient, number, configuration, and type of joints. These results suggest a design principle for the trunk mechanism of a quadruped robot in order to obtain robust and directive locomotion without requiring sensors and actuators.

Keywords: quadrupedal locomotion, walking over rough terrain, vertebrae-inspired trunk mechanism

1. Introduction

Compared to bipedal locomotion, quadrupedal locomotion involves a wider variety of locomotion types such as crawling and bouncing. It is also employed in various types of terrain, such as rough terrain and slopes, as well as in flat planes. In a research area focusing on dynamic locomotion, such as bouncing [1–6], it is assumed that the robot walks on flat plane. Locomotion on rough terrain or slope is another important research area [7–12]. In contrast to a flat plane, the landing position and posture of the foot on rough terrain changes according to the landform; therefore the posture of the entire body changes, which causes falling down or a change to the traveling direction. In order to avoid falling down and achieve *directive locomotion*, in which a robot walks in the correct traveling direction, current research studies adopt dedicated sensing and actuation to measure internal or external information and to direct motion based on the acquired information. Rebula et al. utilized motion capture cameras, at a

distance from the robot, in order to determine the appropriate landing positions, which prevent falling down and provide guidance regarding the correct traveling direction [8]. Considering the limitation of volumetric capacity and the computational resources of autonomous systems, many sensors occupy a large ratio of the capacity and resource, and a lot of sensors have higher probability of mechanical failure. Some studies have adopted a central pattern generator (CPG) using signals from gyro sensors or joint angle sensors, in order to achieve rhythmic locomotion on rough terrain using a simpler sensor set [10, 13]. In order to detect the landing signal of a swinging foot and to measure the state of the robot, such as the posture of the body, which is fetched into the CPG module, a touch sensor, force sensors, gyro sensors, and/or joint angle sensors are generally attached to the robot. Although CPG is one of the candidates to generate adaptive behavior on rough terrain, similar to the former approach, sensors which detect foot landing or measure the posture of the robot, prevent the sustainability of the robot. Many quadruped and hexapod robots are equipped with elastic materials on their legs [9, 10, 14] in order to fit the shape of the terrain. However, because a leg cannot follow a planned trajectory if the deformation volume of the elastic material is too large, the leg including elastic materials cannot correspond to a larger amount of the rough terrain's vertical interval.

For animal locomotion which achieves successful directive locomotion even on rough terrain, not only the legs but also the trunk posture including twisting and rotating is adaptively changed. We assume that the trunk's adaptive behavior is obtained mechanically without a sensor brain or reflection system. When a part of front or rear legs touches on a convex or concave at landing, trunk joints rotates passively and both front and rear legs touch on the ground adaptively in order to support the body without requiring sensors. In this study, we propose a body design for adaptive locomotion on rough terrain. We adopt an animal-like trunk mechanism, which is supported by the redundant and viscoelastic joints of the spine. Some studies have discussed the effect of a trunk mechanism with single or multiple viscoelastic joints. The researchers mainly focused on dynamic lo-



comotion on a flat plane, such as bouncing [2, 15–17], and its analysis [3]. It is expected that the trunk's well-tuned viscoelastic joints will facilitate robust and directive locomotion without requiring the use of sensors and actuators. Turlapati et al. linked multiple modular robots with elastic joints and demonstrated that the linked modular robots could locomote over obstacles [18]. However, the robot had wheels, and the experiment was performed on a two-dimensional plane. For a quadruped robot on three dimensional rough terrain, we observed the advantage of the trunk mechanism with viscoelastic mono- or multi-axial joints over the mechanism of a rigid body. We also observed the influence of joint viscoelasticity, joint configuration, and rotational axis of the joint for successful locomotion. It has been have reported that a robot equipped with a viscoelastic trunk mechanism performs better [19]; this paper focuses on walking performance depending on mechanical design such as the position of joints and the direction of rotational axis with fixed motor command such as the duration of walking cycle and locus of the foot.

The rest of the paper is organized as follows: the design of the quadruped robot equipped with an animal-like trunk mechanism is explained in Section 2. Experiments in order to observe the success rate depending on the amount of viscoelasticity, the joint configuration and rotational joint type are described in Section 3. Finally, the conclusions of this study are presented in Section 4.

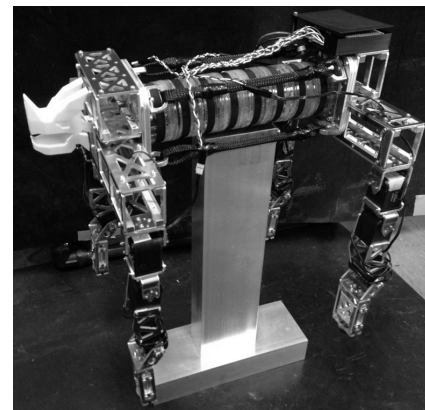
2. Quadruped Robot Configuration

Figure 1(a) shows the prototype of a quadruped robot named Quadrunck; **Fig. 1(b)** shows a screenshot of the simulation based on the physical prototype. **Fig. 2** shows a simulation model. Each leg has a hip (roll and pitch joint, whose rotation axes intersect at a point) and a knee (pitch) joints. The simulation platform used is the Open Dynamics Engine [a]. Unlike the present quadruped models, the robot has up to three viscoelastic joints on the trunk. This section explains the configuration of the quadruped robot including the leg configuration, gait pattern, trunk configuration and trunk mechanism, which provides robust and directive locomotion without requiring sensing and actuation.

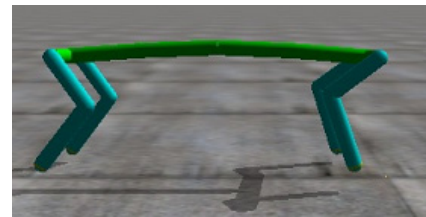
2.1. Leg Configuration and Gait Pattern

As shown in **Fig. 2**, each leg has two links. Trunk and upper link are connected by roll and pitch joints, and the upper and bottom links are connected by a pitch joint. The axes of the roll and pitch joints at the upper position intersect at a point. Based on the physical prototype, the length of the upper and bottom links l_1 and l_2 are 0.15 m and 0.18 m, respectively. The masses of the upper and bottom links are 0.3 kg and 0.2 kg, respectively. The distance between fore and rear legs l_3 is 0.6 m.

A spring damper model is adopted as the contact model between a foot and the ground toward the vertical direction (see **Fig. 3**). The aim of this study is to observe the



(a) Physical prototype



(b) Screenshot of the simulation

Fig. 1. Physical and simulation model of the quadruped robot.

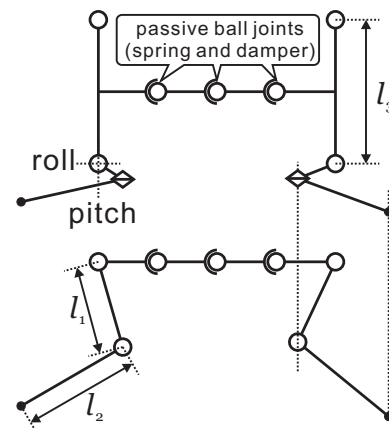


Fig. 2. Schematic design of quadruped robot equipped with trunk mechanism.

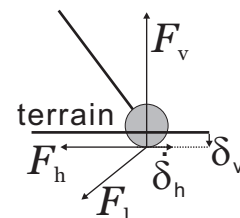


Fig. 3. Contact model.

adaptive static posture according to the shape of ground surface rather than according to dynamic motion; therefore, in order to prevent sliding sideways and back and forth, a simple friction model, Coulomb with viscous frictions, are adopted toward the horizontal directions. The

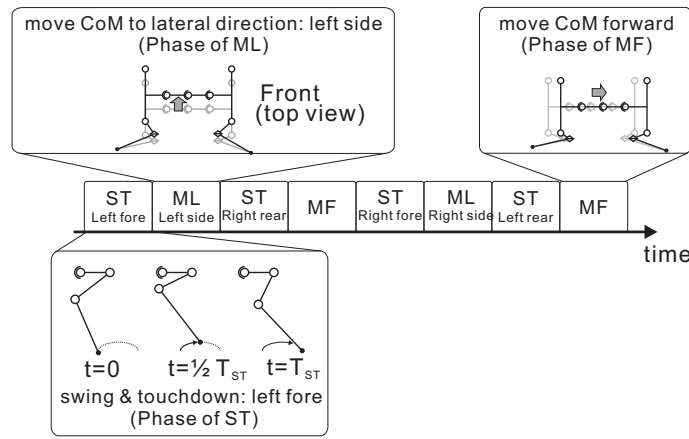


Fig. 4. Gait pattern.

shape of the foot is a ball, and the forces toward the vertical, horizontal, and lateral directions, F_v , F_h , and F_l are expressed as;

$$\begin{cases} F_v = \begin{cases} -K_p \delta_v - K_d \dot{\delta}_v & \text{if } \delta_v < 0, \dot{\delta}_v < 0 \\ -K_p \delta_v & \text{if } \delta_v < 0, \dot{\delta}_v \geq 0 \\ 0 & \text{else} \end{cases} \\ F_h = -\mu F_v \text{sgn}(\dot{\delta}_h) - D \dot{\delta}_h, \\ F_l = -\mu F_v \text{sgn}(\dot{\delta}_l) - D \dot{\delta}_l \end{cases} \quad (1)$$

where δ_v is the distance from the ground to the bottom of the ball, and $\dot{\delta}_h$ and $\dot{\delta}_l$ are the velocities in the horizontal and lateral directions, respectively. $\text{sgn}(\text{value})$ returns +1 when *value* is positive and vice versa. K_p and K_d are the spring and damping coefficients between the foot and the ground, respectively. μ is the friction coefficient. In this study, they are set at $K_p = 5.0 \times 10^4$ N/m, $K_d = 1.0 \times 10^2$ N/(m/s), $\mu = 0.9$, and $D = 0.01$ N/m/s. In the test trial, we confirmed that the foot did not slide on the ground and that the robot obtained the static posture; however, foot contact on the ground slightly oscillated, although the amplitude was very small, less than 10^{-4} m. It is expected that the oscillation is subdued because of moderate viscosity, i.e., D in Eq. (1). The horizontal forces F_h and F_l in Eq. (1) change discontinuously, when the contact point begins to slide. There is room for argument with regard to a precise contact model such as the compliant contact model [20].

The normal crawl is a type of locomotion. The gait is shown in Fig. 4. The locomotion is segmented into eight phases such as “swing and touch down the leg (ST),” “move the center of mass (CoM) toward lateral direction (ML)” and “move CoM forward (MF).” The periods of each phase are expressed as T_{ST} , T_{ML} , and T_{MF} , respectively. In the ST phase, the trajectory of a foot is designed for reaching the peak height in the middle of the phase ($t = 1/2 T_{ST}$) before touching down. In the ML phase, the roll joints of all legs rotate so that the projection of the CoM on the ground is set within the triangle of the supporting feet except a leg swinging in the next phase. Therefore, the CoM of the robot moves to the left side, when the next swinging leg is the right fore or rear leg and

vice versa. In the MF phase, the CoM moves forward for half of the single step. The joints are controlled by the PD feedback controller to ensure that they follow the planned trajectory. The remarkable point is that the robot does not have any feedback controller except the PD controller of the leg joints. This means that sensors such as the gyro, camera, and touch sensor are not mounted on the robot, and that no actuator is used except the actuator on the leg joints. The periods of ST, ML, and MF in Fig. 4 are all set at 250 ms; i.e., a cycle of locomotion is set at $250 \text{ ms} \times 8 \text{ phases} = 2.0 \text{ s}$. The step length is set at 0.2 m, the apex height of the foot at $t = 1/2 T_{SL}$, in the phase of ST, is set at 0.1 m interpolated by a sinusoidal function such as;

$$x = -0.1 \cos\left(\pi \frac{t}{T_{ST}}\right) \dots \dots \dots (2)$$

$$z = 0.1 \sin\left(\pi \frac{t}{T_{ST}}\right), \dots \dots \dots (3)$$

where x is a foot position from the projection of the hip joint on the ground at $t = 0$, according to the direction of the locomotion, and z corresponds with the height of the foot based on the ground. Referring to the foot position, the joint angles of each leg are calculated by inverse kinematics. This paper focuses on the mechanical design of a quadruped robot, and we observed the walking performance of different trunk mechanism designs with common motor command such as the foot trajectory and durations.

2.2. Trunk Configuration

Figure 5 shows the schematic designs of the trunk mechanism. For the purpose of comparing the locomotion influenced by the number, configuration, and rotational axis of the trunk joints, eleven types of trunk mechanism were provided. A trunk has three viscoelastic ball joints (Type A), two joints (Type B–D), one joint (Type E–G), three roll joints (Type H), pitch joints (Type I), yaw joints (Type J), and a rigid body (Type K). The link is cylindrical, and the ball joint is constructed with roll, pitch and yaw joints which intersect at a point. The viscoelasticity model of all

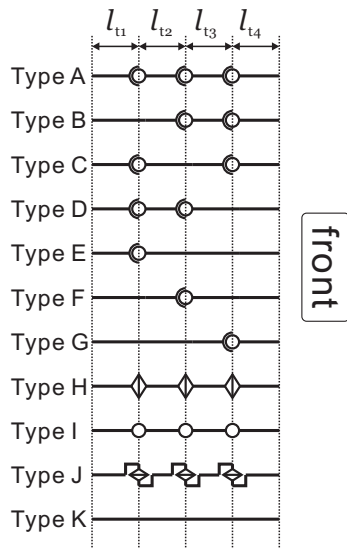


Fig. 5. Eleven types of trunk mechanism (side view).

the joints is expressed as

$$\tau_{ij} = -\widehat{K}_p \theta_{ij} - \widehat{K}_d \dot{\theta}_{ij}, \dots \dots \dots (4)$$

where i indicates the number of joints ($i = 1, 2, 3$ in the case of Type A, for example), j indicates the type of the joint ($j = roll, pitch, yaw$), θ_{ij} is the angle of the joint, and \widehat{K}_p and \widehat{K}_d are the spring and damping coefficient, respectively. The length and weight of each link of Type A, $l_{t1}-l_{t4}$ are identical: 0.2 m and 0.5 kg. The weights of the links of Type B to K are proportional to their lengths. For example, the length and weight of the rear link of Type E are 0.2 m and 0.5 kg, respectively; the length and weight of the front link are 0.6 m and 1.5 kg, respectively.

2.3. Trunk Mechanism for Robust and Directive Locomotion

To explain the capability of robust and directive locomotion, in rough terrain, by utilizing viscoelastic joint(s) in the trunk mechanism, the kinetic balance of the joints in the frontal and top views is explained. Note that only statics are explained in this paper; the investigation of dynamics will be discussed in future work.

- Robustness

Quinn et al. pointed out an important role of the body flexion joint; they developed Whegs II, a hexapod robot [21]. Some studies have equipped a legged robot with a leg made of elastic materials or a series elastic actuator. For example, Hutter et al. adopted a series elastic actuator (SEA) [22]. By using SEA, it is expected that the robot achieves an adaptive landing posture according to the shape of the rough terrain. In general, from a kinematics viewpoint, a joint at a distance from the foot provides larger movable range to the foot than does a joint closer to the foot. Although the flexible leg addresses a convex by passively changing the posture of the leg without sensors, it requires some sensors to detect a foot landing

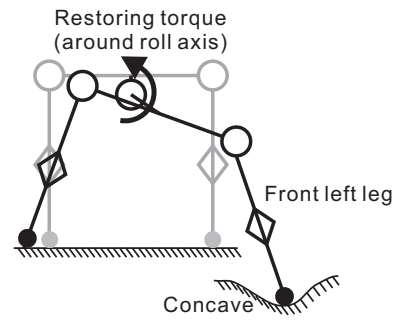


Fig. 6. Supplemental force to lift up the leg on a concave surface.

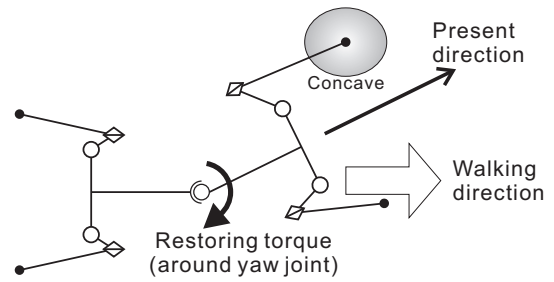


Fig. 7. Restoring force for directive locomotion.

for stretching the leg when the foot lands on a concave. On the other hand, by embedding joint(s) in the trunk, the movable range is larger because the position of the joint is at a distance from the foot, and the foot lands on the concave by rotating the trunk joint mechanically without sensors. Fig. 6 shows the case of where the left foreleg is lifted by contacting a concave surface. As shown in the figure, when the trunk has an elastic joint, torque around the roll axis of the trunk joint acts as a supplemental force to lift up the leg; therefore, the robot can achieve robust locomotion on a concave surface. Although supplemental force occurs in the rigid trunk while the foot is lifted up, the rigid body does not deform according to the height of the terrain; therefore, the foot does not land on the concave.

- Directivity

Figure 7 shows the same case discussed previously. As shown in the figure, the direction of the locomotion is changed, and a torque is added around the yaw axis of the trunk joint as a force to restore the forward direction of locomotion.

3. Experiment

3.1. Observation of Restoring Torques

As explained in Section 2, roll, pitch, and yaw joints are expected to generate the restoring force for stable and directive locomotion. Before explaining experiments, we observe the force around each joint. In order to observe

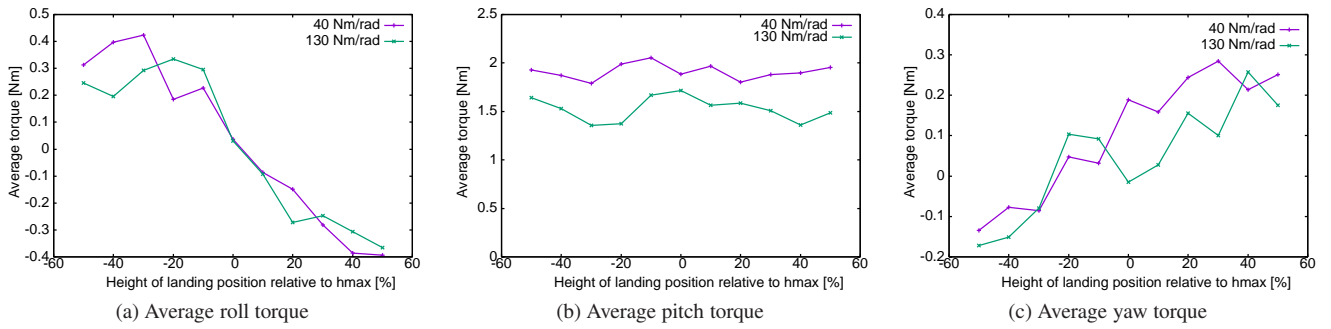


Fig. 8. Average torque of Type F at $K_p = 40$ and 130 Nm/rad.

the restoring torque shown in Figs. 6 and 7, the average torques of the roll, pitch, and yaw joints of the Type F single joint set were recorded. The robot walked on a flat plane for some steps, and the height of the landing position of the left foreleg was changed from -50% (concave) to $+50\%$ (convex) on the basis of h_{max} , which was the height from a base line when the time in each swing phase was $t = 1/2T_{st}$ in the ST phase. After one cycle, the height of the landing position was set to zero. The torques were then recorded for two cycles and the average torque around each joint was calculated as;

$$\bar{\tau}_i = \frac{1}{N} \sum_j \tau_{ij}, \quad i = roll, pitch, yaw, \quad j = 1, 2, \dots, N \quad (5)$$

where N is the number of recorded values.

Figure 8 shows the average torques following Eq. (5) of Type F when the elastic coefficient was set to 40 and 130 Nm/rad. When τ_{roll} in Eq. (5) was positive, the frontal part of the trunk rotated counterclockwise, relative to Fig. 6. When τ_{pitch} was positive, the frontal part of the trunk inflected. When τ_{yaw} was positive, the direction of the front part rotated toward the left. The horizontal axis indicates the height of the convex or concave (negative: concave and positive: convex) surface. When the left foreleg landed on the concave surface, the roll joint of the trunk passively rotated clockwise as shown in Fig. 6; the yaw joint rotated counterclockwise as shown in Fig. 7 and vice versa. The pitch angle always extended to resist gravity. As shown in Fig. 8, the roll, pitch, and yaw torques were added against the direction of passive rotation to restore the posture; therefore, as mentioned above, the torques of the elastic trunk help prevent falls and changes in direction; thereby, the robot obtained directive locomotion over rough terrain without requiring sensing and actuation.

3.2. Setup

This study observed the effects of various types of trunk mechanism equipped with viscoelastic joints and compared them with the conventional rigid body trunk mechanism. The robot has four legs driven by three joints in each leg, following a typical trajectory by the PD controller. It does not have any sensors measuring the angles of trunk joints, posture of the robot, or the position of the

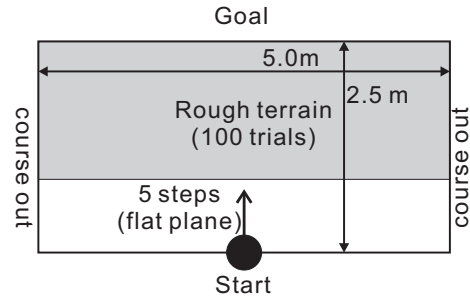


Fig. 9. Field for validation.

landing foot. The trunk joint(s) are not controlled but are passively rotated around the roll, pitch, and yaw axes following the spring-damper model. In order to evaluate the advantage of the proposed trunk mechanism in comparison to the currently used rigid body design, success and failure rates according to trunk’s joint stiffness on various types of rough terrain were observed in the simulation.

A field for validation is shown in Fig. 9. The width of the field is 5.0 m. The robot walked 5 steps on a flat plane and then walked over various types of rough terrain constructed randomly. When the robot stepped outside the field, it was recorded as “Course Out (CO)” which was a locomotion failure. When the robot either fell down or walked for a duration of over 100 s, the event was also recorded as a failure (“Fall Down (FD)” and “Time Over (TO),” respectively). When the robot walked over 2.5 m without CO, FD or TO, it was recorded as “Successful Locomotion (SL).”

In this section, the success and failure rates of the robot equipped with Type A and K, observed in order to compare the locomotion ability on various types of rough terrain, are explained. In the case of Type A, the elastic coefficient \widehat{K}_p in Eq. (4) was changed from 10 to 100 Nm/rad by 10 Nm/rad, and changed from 100 Nm/rad by 100 Nm/rad. The viscous coefficient was fixed at 0.01 Nm/(rad/s). Each trunk mechanism was evaluated using a stochastic approach: a robot equipped with each trunk type and with each elastic coefficient undergoing 100 trials in 100 types of rough terrain; success rates of SL, CO, TO, and FD were recorded. Because Type K does not have a joint, the robot equipped with the rigid

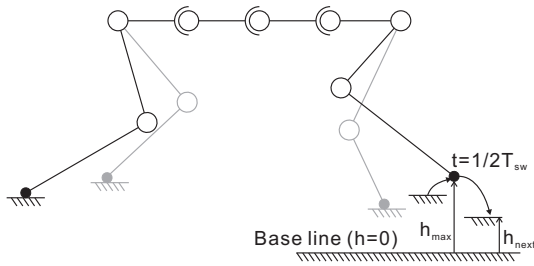


Fig. 10. Determination of the landing height.

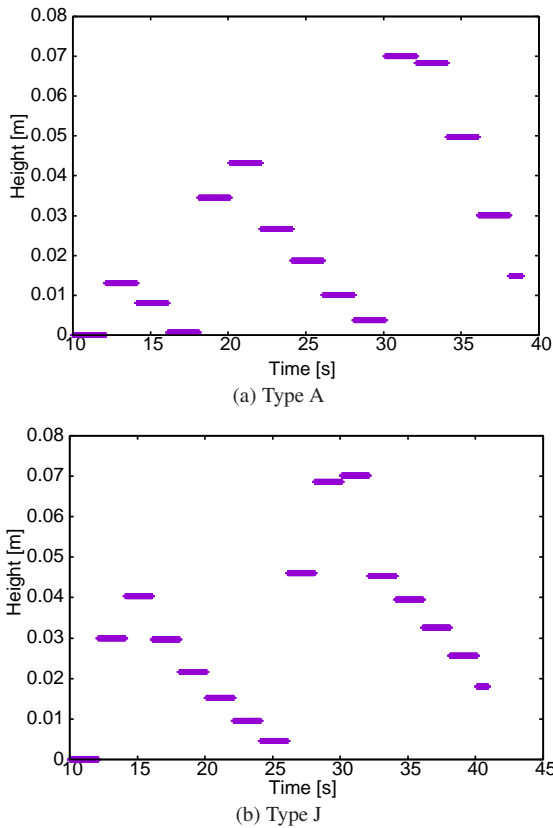


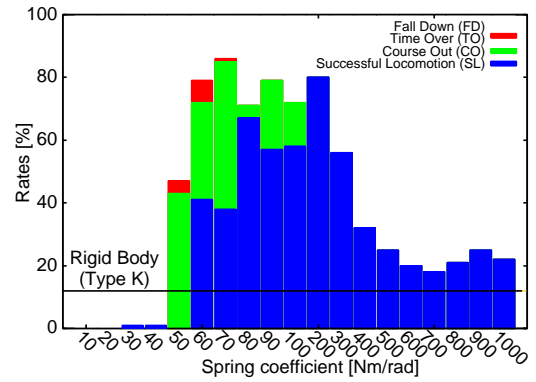
Fig. 11. Examples of a time sequence of the height of the terrain.

body had 100 trials. Fig. 10 shows the procedure for determining the landing height of the swinging leg in order to generate various types of rough terrain. In each SL phase, the height of the contact point for landing h_{next} was determined as

$$h_{next} = rand \times h_{max},$$

where $rand$ is a random value between 0.0 and 0.5; i.e., the height of the terrain for landing was randomly determined from 0% to 50% of h_{max} . The base line was set at zero when the robot began to walk.

Figure 11 shows time sequence examples of the terrain height for the left foreleg, when the model was equipped with Type A and J. The landing terrain for each leg was a plane, and the height of the landing terrain was changed randomly. As shown in the figures, the heights were less than 0.1 m, which is the maximum height of the foot in



(a) Rates on Type A and Type K

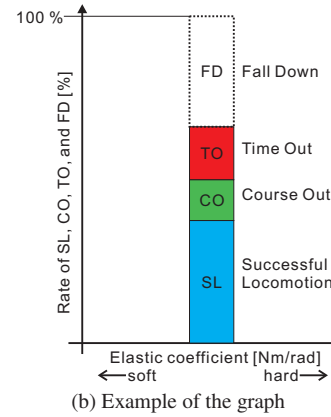


Fig. 12. Rates of SL, CO, TO, and FD according to elastic coefficient \widehat{K}_p .

the ST phase (see Fig. 4); the variance of the height is almost the same for each trunk type.

3.3. Results

The Type K robot equipped with the rigid trunk succeeded 12 times and fell down 88 times over 100 trials; i.e., the success rate of the robot equipped with a rigid body was 12%. Because the robot equipped with the rigid body does not have a redundant joint for adjusting to different ground heights, it is expected to adopt a controller, which determines the loci of the feet; the controller will require some expensive, heavy, and complex sensors such as a motion capture and laser range finder. The rate of SL, CO, and TO of Type A depending on the elastic coefficient and SL of Type K are shown in Fig. 12(a). Fig. 12(b) shows an example of the graph as stacked chars, which explains SL, CO, TO and FD rates from the bottom up at certain elastic coefficient. The blank denotes the FD rate; the time step in the simulation was set to 0.05 ms; the results were obtained over approximately three days (CPU: Intel Core i7 5820K, memory: 32 GB). In Fig. 12(a), the rates of SL, CO, and TO changed depending on the elastic coefficient in the case of Type A. A remarkable point in Fig. 12(a) is that the robot equipped with trunk Type A with appropriate viscoelasticity achieved a higher success rate of locomotion on rough terrain. When the elastic coefficient \widehat{K}_p is smaller than 40 Nm/rad, the robot

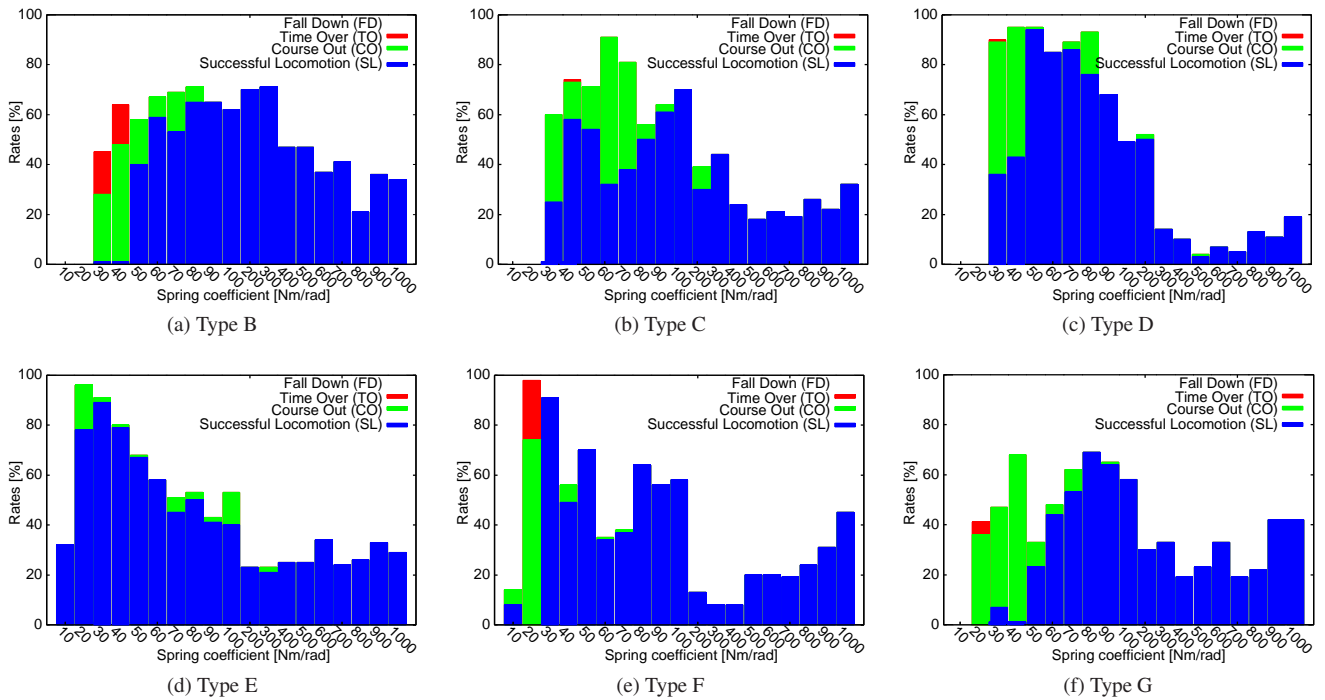


Fig. 13. Rates of SL, CO, TO, and FD of Types B to G.

almost always fell down in every trial. When \widehat{K}_p was set to 50 Nm/rad, the FD rate was smaller; however, the robot did not reach the goal but rather walked toward the wrong direction. When \widehat{K}_p was set from 60 Nm/rad to 100 Nm/rad, the rate of SL was over 35%; however, the robot could not reach the goal in some trials. When \widehat{K}_p was set from 200 Nm/rad to 300 Nm/rad, the robot achieved a higher SL rate, over 70% without walking toward the wrong direction. Especially when it was set to 200 Nm/rad, the SL rate was highest, at 80%, which is 6 times more than the case of the rigid body. When \widehat{K}_p was set over 400 Nm/rad, SL rates were almost the same as Type K. This result showed that compliant trunk joints provide stable locomotion; when the stiffness was appropriately set between 200 and 300 Nm/rad, direction change was compensated by moderately restoring the joint force as well as by adjusting the joints according to the shape of the ground in order to avoid falling down.

3.4. Contribution of Position and Rotational Axis

Among three ball joints including roll, pitch, and yaw joints, we should know (1-1) how many ball joints, (1-2) which position of the ball joint(s), and (1-3) which rotational axis contributes to stable and directive locomotion. This information helps not only in understanding the trunk mechanism’s design principle but also in constructing the physical trunk mechanism because it is difficult to realize a ball joint, whose joint spring coefficients around the roll, pitch and yaw axis are tunable. Then we observed the success rate of each joint mechanism. For (1-1) and (1-2), the rates of Type B to G in Fig. 5 were observed. For (1-3), the rates of Type H to J were observed.

3.4.1. Success Rates by Position of the Ball Joints

Figure 13 shows the success rate results of Types B to G, whose number of joints and position of the joint were different. The experimental setup is the same as in the case described in the previous section. The distributions of SL, CO, TO, and FD depend on trunk types.

These results indicate some interesting trunk design options. One of them is that the distribution of rates varies according to the position of joints, even if the number of joints is the same (two joints: Type B–D, single joint: Type E–G). Because the viscosity \widehat{K}_d is constant, the total amount of the whole body’s viscosity is fixed with respect to the joint number in the cases of trunk Type A to G. The stability of the locomotion depends on the viscosity and elasticity of the trunk. These results show that not only the total amount of viscosity and elasticity but also position of the joints influence the stability of locomotion. In this study, the viscosity was fixed due to the limitation of the vast range of exploration. We should discuss the influence of the viscosity as well as elasticity.

Another option is that trunks with different number of joints provide similar rate distributions. The robot equipped with Type B and G achieved higher CO and TO rates, when the spring coefficient was smaller (Type B: 30–40 Nm/rad, and Type G: 20–40 Nm/rad). When the spring coefficient was higher than 50 Nm/rad, the rate of SL was higher, although the SL rate did not reach 80%, which is the maximum SL rate in the case of Type A. The robot equipped with Type F achieves a higher rate of SL, over 80%, when the spring coefficient was tuned at 30 Nm/rad. However, the rate was zero if the spring coefficient was slightly misaligned at 20 Nm/rad. The

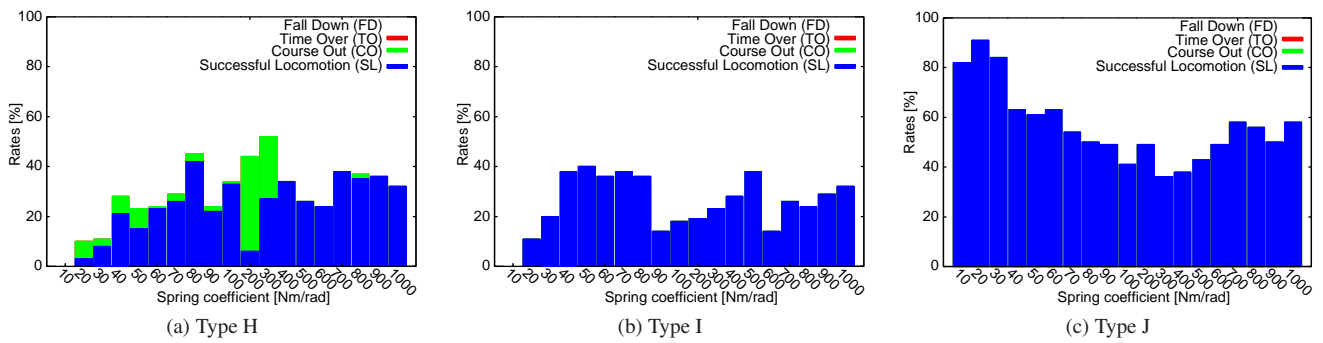


Fig. 14. Rates of SL, CO, TO, and FD of Types H to J.

robot equipped with Type C achieved some degree of SL rate even when the spring coefficient was smaller, at 30–40 Nm/rad, by which Type B and G did not provide SL. However, the rate of SL was not much higher than 80%. The robot equipped with Type D and E achieved a higher SL rate of approximately 80%, when the spring coefficient was appropriately tuned (Type D: 50–70 Nm/rad, and Type E: 20–40 Nm/rad). As shown in Fig. 5, Type B and G have the joint(s) at the frontal position and Type F has the joint at the middle position. Type C has the joints at the rear position as well as the frontal position. Type D and E do not have the joint at the frontal position but rather at the rear position. These results suggest that the trunk embedding the joint in the frontal position does not improve performance (Type B and G) and that the trunk embedding the joint in the rear position improves performance (Type D and E).

3.4.2. Success Rates by Rotational Axis Type of Trunk Joints

Although the trunk including ball joints with appropriate spring coefficient achieves successful locomotion on rough terrain, it is technically difficult to realize a physical viscoelastic ball joint in which the viscoelastic roll, pitch and yaw joints intersect at a point. Therefore, in order to obtain a simpler joint mechanism, we investigated which rotational axis contributes to stable and directive locomotion. Then, as shown in Fig. 5, we adopted Type H, I, and J, as the trunk mechanism and observed SL, CO, FD, and TO rates according to each trunk mechanism's spring coefficient. The simulation setup is the same as the one described in the previous section.

Figure 14 shows the relationships between the spring coefficient of the joints and success/failure rates. Figs. 14(a), (b), and (c) show the relationship in the case where the trunk joints rotate around the roll, pitch and yaw axis, respectively. As shown in Figs. 14(a) and (b), the robot could not obtain a higher SL rate, even if the spring coefficient was tuned. On the other hand, as shown in Fig. 14(c), the trunk mechanism including three yaw joints achieved higher success rate. Especially, when the spring coefficient was set at 20 Nm/rad, the SL rate was highest at 88%, which is higher than the case of Type A in which the spring coefficient was tuned at 200 Nm/rad.

Because Type J does not include roll joints, the trunk cannot twist and the robot cannot obtain the posture as shown in Fig. 6. A detailed investigation of the trunk mechanism containing only yaw joints will be carried out in future work.

4. Conclusion

This study observed the effects of various types of trunk mechanisms, with embedded viscoelastic joints, and compared them with the conventional trunk mechanism of the rigid body. The robot has four legs driven by three normal joints in each leg, which follow a typical trajectory. It does not have any sensors measuring the angles of trunk joints, posture of the robot, or position of the landing foot. The trunk joint(s) were not controlled but passively rotated around the roll, pitch, and yaw axes following the spring-damper model.

First, we observed that the torques, which restore the trunk joint in order to prevent falls and achieve directive locomotion were appropriately applied. Second, joint elasticity was varied and the success rates of 100 trials, for each elastic coefficient and joint configuration, were recorded. We found that the trunk mechanism with appropriate elastic joints had a higher success rate than the rigid body. Third, we found that success rate distribution varied with the position and the axis of the joint.

As mentioned above, the robot equipped with a rigid body realized successful locomotion over rough terrain by using sensors such as a touching, gyro, and camera sensors, and a precise controller, which plans the foot trajectory, in response to the sensor information for example. On the other hand, we did not adopt a sensor and controllers which changes motor command such as step width, step height, and duration of each phase. This approach refers to morphological computation [23]. Morphological computation claims that the motion occurs by an interaction between a system including mechanical structure and an environment such as terrain. Following this approach, we assumed that the robot achieves successful locomotion even with “cheap” motor command and controller. This study partly demonstrated that a robot equipped with a well-designed trunk mechanism achieves

better locomotion performance.

This is a first step toward investigating the effect of joints on the trunk; the dynamics of the trunk will be considered in future work. The dynamics of locomotion will reveal a design principle including the size, mass, and position of viscoelastic joints. They will also explain a class of the rough terrain, i.e., how much the depth and height of concave and convex can correspond to the arbitrary size and mass of the robot. One of the factors providing successful locomotion is the feet's range of motion. We found that the robot obtains stable posture not only by rotating the trunk joints but also by the slipping and pivoting of the feet. Therefore, in order to investigate locomotion stability, we should consider not only the motion space but also slipping and pivoting.

From the results shown in **Figs. 12(a) to 14(c)**, we found that the SL rate changes according to the spring coefficient. These results suggest that the natural frequency of the robot influences the rate of SL. Some studies have reported an energy efficient behavior, such as jumping [24], by tuning an actuation frequency. This study focuses on the stability of locomotion rather than on energy efficiency; therefore, careful discussion is needed with regard to natural frequency providing successful locomotion over rough terrain. In the case of animals, we assume that the stiffness of the trunk joint switches by changing the degree of myotony. Although there are some papers, which report the measurement of human and animal muscle activity [25], it is very difficult to measure the stiffness of living trunk joints directly. One of the advantages of biologically-inspired robots is the capability of assuming such phenomena by measuring the robot directly. We are now designing and conducting a trial run with a physical quadruped robot equipped with the trunk mechanism. Simulation validation experiments using the physical robot will be described in future work.

References:

- [1] Q. Cao, A. T. van Rijn, and I. Poulakakis, "On the control of gait transitions in quadrupedal running," 2015 IEEE/RSJ Int. Conf. on Intelligent Robots and Systems (IROS), pp. 5136-5141, 2015.
- [2] U. Çulha and U. Saranlı, "Quadrupedal bounding with an actuated spinal joint," 2011 IEEE Int. Conf. on Robotics and Automation (ICRA), pp. 1392-1397, 2011.
- [3] R. Yamasaki, Y. Ambe, S. Aoi, and F. Matsuno, "Quadrupedal bounding with spring-damper body joint," 2013 IEEE/RSJ Int. Conf. on Intelligent Robots and Systems (IROS), pp. 2345-2350, 2013.
- [4] S. Makita, D. Nishimura, and J. Furusho, "Development of horse-type quadruped robot (report2, experiments of trot gait by quadruped robot PONY)," J. of Robotics and Mechatronics, Vol.16, No.1, pp. 104-112, 2004.
- [5] K. Nakada, T. Asai, and Y. Amemiya, "Biologically-inspired locomotion controller for a quadruped walking robot: Analog ic implementation of a cpg-based controller," J. of Robotics and Mechatronics, Vol.16, No.4, pp. 397-403, 2004.
- [6] J. G. Nichol, S. P. N. Singh, K. J. Waldron, III L. R. Palmer, and D. E. Orin, "System design of a quadrupedal galloping machine," The Int. J. of Robotics Research, Vol.23, No.10-11, pp. 1013-1027, 2004.
- [7] M. Raibert, K. Blankespoor, G. Nelson, R. Playter, and the Big-Dog Team, "Bigdog, the rough-terrain quadruped robot," 17th World Congress The Int. Federation of Automatic Control (IFAC), pp. 10822-10825, 2008.
- [8] J. R. Rebula, P. D. Neuhaus, B. V. Bonlander, M. J. Johnson, and J. E. Pratt, "A controller for the littledog quadruped walking on rough terrain," 2007 IEEE Int. Conf. on Robotics and Automation (ICRA), pp. 1467-1473, 2007.
- [9] A. Sorocowicz, L. Kuechler, A. Tuleu, M. Ajalloeian, M. D'Haene, R. Moeckel, and A. J. Ijspeert, "Oncilla robot – a light-weight bio-inspired quadruped robot for fast locomotion in rough terrain," Fifth Int. Symposium on Adaptive Motion of Animals and Machines, pp. 63-64, 2011.
- [10] Y. Fukuoka, H. Katabuchi, and H. Kimura, "Dynamic locomotion of quadruped tekken 3 & 4 using simple navigation," J. of Robotics and Mechatronics, Vol.22, No.1, pp. 36-42, 2010.
- [11] C. Gehring, C. D. Bellicoso, S. Coros, M. Bloesch, P. Fankhauser, M. Hutter, and R. Siegwart, "Dynamic trotting on slopes for quadrupedal robots," 2015 IEEE/RSJ Int. Conf. on Intelligent Robots and Systems (IROS), pp. 5129-5135, 2015.
- [12] Z. G. Zhang, H. Kimura, and Y. Fukuoka, "Self-stabilizing dynamics for a quadruped robot and extension toward running on rough terrain," J. of Robotics and Mechatronics, Vol.19, No.1, pp. 3-12, 2007.
- [13] M. Ajalloeian, S. Pouya, A. Sproewitz, and A. J. Ijspeert, "Central pattern generators augmented with virtual model control for quadruped rough terrain locomotion," 2013 IEEE Int. Conf. on Robotics and Automation (ICRA), pp. 3321-3328, 2013.
- [14] U. Saranlı, M. Buehler, and D. E. Koditschek, "RHex: A simple and highly mobile hexapod robot," The Int. J. of robotics research, Vol.20, No.7, pp. 616-631, 2001.
- [15] X. Wei, C. Wang, Y. Long, and S. Wang, "The effect of spine on the bounding dynamic performance of legged system," Advanced Robotics, Vol.29, No.15, pp. 973-987, 2015.
- [16] T. Takuma, M. Ikeda, and T. Masuda, "Facilitating multi-modal locomotion in a quadruped robot utilizing passive oscillation of the spine structure," Proc. of the 2010 IEEE/RSJ Int. Conf. on Robotics and Automation (IROS), pp. 4940-4945, 2010.
- [17] Q. Cao and I. Poulakakis, "Quadrupedal bouncing with a segmented flexible torso: passive stability and feedback control," Bioinspiration & Biomimetics, Vol.8, No.4, 046007, 2013.
- [18] S. H. Turlapati, M. Shah, S. P. Teja, A. Siravuru, S. V. Shah, and K. M. Krishna, "Stair climbing using a compliant modular robot," 2015 IEEE/RSJ Int. Conf. on Intelligent Robots and Systems (IROS), pp. 3332-3339, 2015.
- [19] T. Takuma and W. Kase, "Robust and directive quadruped locomotion on rough terrain without requiring sensing and actuation," Proc. of the 2015 IEEE Int. Conf. on Robotics and Biomimetics (ROBIO), page SuD04.4, 2016.
- [20] P. R. Kraus and V. Kumar, "Compliant contact models for rigid body collisions," Proc. of the 1997 IEEE Int. Conf. on Robotics and Automation (ICRA), pp. 1382-1387, 1997.
- [21] R. D. Quinn, G. M. Nelson, R. J. Bachmann, D. A. Kingsley, J. T. Offi, T. J. Allen, and R. E. Ritzmann, "Parallel complementary strategies for implementing biological principles into mobile robots," The Int. J. of Robotics Research, Vol.22, No.3-4, pp. 169-186, 2003.
- [22] M. Hutter, C. D. Remy, M. A. Hoepflinger, and R. Siegwart, "Efficient and versatile locomotion with highly compliant legs," IEEE/ASME Trans. on Mechatronics, Vol.18, No.2, pp. 449-458, 2013.
- [23] R. Pfeifer, F. Iida, and G. Gómez, "Morphological computation for adaptive behavior and cognition," Int. Congress Series, Vol.1291, pp. 22-29, 2006.
- [24] J. Aguilar, A. Lesov, K. Wiesenfeld, and D. I. Goldman, "Lift-off dynamics in a simple jumping robot," Physical Review Letters, Vol.109, No.17, 174301, 2012.
- [25] S. Valentin and T. F. Licka, "Spinal motion and muscle activity during active trunk movements – comparing sheep and humans adopting upright and quadrupedal postures," PLoS ONE, Vol.11, No.6, e0146362, 2016.

Supporting Online Materials:

- [a] ODE Home Page: <http://www.ode.org/>
[Accessed June 1, 2017]



Name:
Takashi Takuma

Affiliation:
Osaka Institute of Technology

Address:

5-16-1 Omiya, Osaka 535-8585, Japan

Brief Biographical History:

1999 Received B.E. in Engineering Science from Osaka University
2001 Received M.Eng. in Informatics from Kyoto University
2006- Research Associate, Osaka University
2008- Assistant Professor, Osaka Institute of Technology
2013- Associate Professor, Osaka Institute of Technology

Main Works:

- H. Oku, N. Asagi, T. Takuma, and T. Masuda, "Passive Trunk Mechanism for Controlling Walking Behavior of Semi-passive Walker," 2015 IEEE/RSJ Int. Conf. on Intelligent Robots and Systems (IROS), 2015.
- T. Takuma, K. Takamine, and T. Masuda, "Sensing Mechanism for Estimation of the Physical Properties of an Object avoiding Failure of the Sensors," Advanced Robotics, Vol.28, Issue 16, pp. 1055-1066, 2014.
- T. Takuma, R. Izawa, T. Inoue, and T. Masuda, "Mechanical Design of a Trunk with Redundant and Viscoelastic Joints for Rhythmic Quadruped Locomotion," Advanced Robotics, Vol.26, pp. 745-764, 2012.

Membership in Academic Societies:

- The Robotics Society of Japan (RSJ)
- The Japanese Society of Mechanical Engineers (JSME)
- The Society of Instrument and Control Engineers (SICE)
- The Institute of Electrical and Electronics Engineers (IEEE)



Name:
Wataru Kase

Affiliation:
Osaka Institute of Technology

Address:

5-16-1 Omiya, Osaka 535-8585, Japan

Brief Biographical History:

1985/1987/1990 Received B.E., M.E. and Ph.D. degrees from Sophia University
1990- Research Associate, Department of Information Engineering, Nagoya University
1996- Joined Department of Electrical and Electronic Systems Engineering, Osaka Institute of Technology
2007- Professor, Osaka Institute of Technology

Main Works:

- W. Kase, "A simple derivation of the right interactor for a tall transfer function matrix and its application to inner-outer factorization," Electronics and Communications in Japan, Vol.95, No.8, pp. 17-25, 2012.
- W. Kase and Y. Shigehiro, "Pseudo Innerizing Control by State Feedback," IEEEJ Trans. on Electronics, Information and Systems, Vol.136, pp. 1827-1833, 2016.

Membership in Academic Societies:

- The Institute of Electrical Engineers of Japan (IEEJ)
- The Society of Instrument and Control Engineers (SICE)
- The Institute of Systems, Control and Information Engineers (ISCIE)
- The Institute of Electrical and Electronics Engineers (IEEE)



Name:
Yoshiki Murata

Affiliation:
Osaka Institute of Technology

Address:

5-16-1 Omiya, Osaka 535-8585, Japan

Brief Biographical History:

2017 Received Bachelor degree from Osaka Institute of Technology
2017- Master Course Student, Osaka Institute of Technology

Main Works:

- biologically inspired quadruped robot